Materials Research Express

PAPER

Effect of the dopant on the structural and hyperfine parameters of $Sn_{0.95}M_{0.05}O_2$ nanoparticles (M: V, Mn, Fe, Co)

To cite this article: V Bilovol *et al* 2019 *Mater. Res. Express* **6** 0850h6

Materials Research Express

PAPER

Effect of the dopant on the structural and hyperfine parameters of $Sn_{0.95}M_{0.05}O_2$ nanoparticles (M: V, Mn, Fe, Co)

V Bilovol[1,2], S Ferrari[1,2], F D Saccone[3,4] and L G Pampillo[1,2]

[1] Universidad de Buenos Aires. Facultad de Ingeniería. Laboratorio de Sólidos Amorfos. Av. Paseo Colón 850, C1063ACV, Ciudad Autónoma de Buenos Aires, Argentina
[2] CONICET—Universidad de Buenos Aires. Instituto de Tecnologías y Ciencias de la Ingeniería 'Hilario Fernández Long' (INTECIN). Buenos Aires, Argentina
[3] Universidad de Buenos Aires, Facultad de Ingeniería, Departamento de Física. Av. Paseo Colón 850, C1063ACV, Ciudad Autónoma de Buenos Aires, Argentina
[4] YPF Tecnología S.A., Av. del Petróleo S/N e/129 y 143, Berisso, B 1923, Buenos Aires, Argentina

E-mail: vbilovol@fi.uba.ar

Keywords: Mossbauer spectroscopy, XPS, SnO_2-doped nanoparticles, XRD

RECEIVED 12 April 2019
REVISED 6 June 2019
ACCEPTED FOR PUBLICATION 13 June 2019
PUBLISHED 21 June 2019

Abstract

In this work, we present a comparative study of the structural and hyperfine parameters on tin dioxide nanoparticles doped with different transition metal elements. The nanopowders with the stoichiometry $Sn_{0.95}M_{0.05}O_2$ (M: V, Mn, Fe, Co) were synthesized by simple co-precipitation method. The characterization was carried out by conventional x-ray diffraction technique, transmission ^{119}Sn Mössbauer spectroscopy and x-ray photoelectron spectroscopy (XPS). The effect of dopant element on structural parameters of tin dioxide and, particularly, on hyperfine parameters of Sn was analysed. It was found that dopants, except for Fe, were in two valence states. For the Mn-doped SnO_2 sample, it was found the strongest influence of M cation on Sn hyperfine parameters, whereas Co-doped sample resulted in the least altered one as compared to doped and un-doped SnO_2. We propose an explanation of the changes of the hyperfine parameters observed over the modification of the structural changes, based on the size of the dopant elements, whose oxidation states were identified by XPS. Additionally, it should not be discarded the relevant role of oxygen vacancies whose presence on the surface was indirectly witnessed by XPS.

Introduction

Tin dioxide (SnO_2) is a wide band-gap (about of 3.6 eV for the bulk material at room temperature) n-type semiconductor and a transparent conducting oxide, which has many technological applications related to the combination of its characteristic properties. Therefore, this system has been of great interest in research in recent years. At ambient pressure, SnO_2 has a tetragonal rutile—type structure (low pressure phase, space group $P4_2/mnm$). This structure is composed of chains of edge-sharing SnO_6 octahedral units lying along the *c*-axis with corner-sharing cross linkages along the perpendicular directions.

The incorporation of dopants in the SnO_2 system produces important changes in its properties. For instance, the use of transition metal (TM) elements as dopant has attracted a great attention because of interesting magnetic properties of the doped semiconductor, which makes it a promising candidate as a diluted magnetic semiconductor (DMS) [1, 2].

From other approach, regarding its application as a gas sensor, the incorporation of TM elements changes its sensitivity, selectivity and time response [3]. Besides TM elements, trivalent rare earth (RE) elements are used as dopants because they provide advantageous features without altering the main properties that define the system as a transparent-conducting oxide [4–6]. Additionally, incorporation of a RE element can induce highly attractive optoelectronic properties positioning these materials as possible candidates for the development of different devices such as LEDs and lasers [7].

It is well known that materials in the nanoscale range can exhibit unique properties compared to their bulk counterparts mostly because of the significant ratio surface/volume. In this connection, differences between surface properties and the ones corresponding to the core, are usually found [8]. For instance, conductivity of SnO_2 is very sensitive to the surface state, as well as absorption properties and reactivity [9].

Therefore, a combination of both surface- and bulk-sensitive techniques can result very fruitful giving a more complete information, especially structural, about a nanoparticle (NP) system under research. In this work, we have unified the potentiality of two spectroscopic techniques, ^{119}Sn Mössbauer spectroscopy in transmission geometry and x-ray photoelectron spectroscopy, in addition to the conventional x-ray diffraction technique. We have identified the chemical state of the 3*d* dopants and their impact on SnO_2 NP structural parameters and also on the hyperfine parameters of tin in the host matrix.

Experimental

$Sn_{0.95}M_{0.05}O_2$ nanoparticles (M: V, Mn, Fe, Co) were prepared by the wet chemical co-precipitation method following the procedure described elsewhere in [10]. Here, we only recall the chlorides of the transition metals used for the syntheses: VCl_3, $MnCl_2$, $FeCl_3$ and $CoCl_2$.

Energy dispersive spectroscopy with Oxford Instruments X-MaxN 50 SDD was carried out in order to get insight of the elemental analysis.

Conventional x-ray diffraction was carried out with a Rigaku D/max diffractometer equipped with a vertical goniometer, using a Bragg–Brentano geometry (θ–2θ coupled arms) and Cu-Kα radiation in the $20^\circ \leqslant 2\theta \leqslant 80^\circ$ range, measuring with a 0.05° step and sweeping with a 0.4°/min velocity.

The samples were analyzed by Mössbauer spectroscopy, at room temperature, using the 23.875 keV γ-radiation from a $Ca^{119m}SnO_3$ source with transmission geometry. In all the samples, the isomer shift is reported relative to $CaSnO_3$ at 300 K. The calibration was carried out employing the ^{57}Fe 14.4 keV γ-radiation from a ^{57}Co(Rh) source with sodium nitroprusside as absorber.

FlexPS equip (Specs) was used during the XPS measurements employing a monochromatic *Al* K_α ($h\nu = 1486.6$ eV) source, 100 W power and 10 kV voltage. The scans were acquired with a pass-energy of 20 eV, 20 scans per sample. The instrument work function was calibrated using C1s photoelectron. Spectra were analyzed using *Casa XPS* software. Gaussian (70%)—Lorentzian (30%) profiles were used for fitting core levels. A standard Shirley background was used for all reference sample spectra.

Results

Elemental analysis of the doped SnO_2

The elemental analysis of the doped samples was provided by energy dispersive x-ray spectroscopy (EDX) in order to corroborate their chemical composition. Meanwhile the corresponding results of Fe- and V-doped SnO_2 are mentioned in [11, 12], respectively, here we show EDX results of Co- and Mn-doped SnO_2 samples. The values of 3.8_5 at% for Co and 5.2_9 at% for Mn were estimated being in each case the average of eight inspected zones (for example, figure 1, corresponding to Co-doped SnO_2).

X-ray diffraction technique and transmission ^{119}Sn Mössbauer spectroscopy

Figure 2 shows XRD patterns of Mn- and Co-doped samples, whereas the corresponding ones of Fe and V-doped samples were shown elsewhere [11, 12]. In all the cases, cassiterite SnO_2, which is isomorphic to rutile (space group $P4_2/mnm$) was identified by the diffraction peaks presented in the shown patterns. The absence of secondary segregated phases in the XRD spectra is a good evidence that the doping element was incorporated into the SnO_2 lattice. Rietveld refinements of the experimental diffraction patterns allowed extracting the valuable structural properties of the system under research. In table 1 we show the goodness of the Rietveld refinements.

On base of the extracted lattice parameters *a* and *c*, the volume of the cassiterite lattice (with the individual dopants) was calculated and compared with un-doped SnO_2 one (figure 3). The crystallite size of the doped-SnO_2 samples was under 20 nm. As it can be seen, in all the cases, except for Co-doped SnO_2, doping SnO_2 leads to contraction of the rutile lattice.

Mössbauer spectroscopy is a very powerful technique for studying the local environment of Sn atom in Sn-solid samples because one of the Sn isotopes, ^{119}Sn, is one of the best-suited probes for Mössbauer experiments. The local environment of tin can be described by means of the hyperfine interactions that the atom probe reveals in a solid matrix: isomer shift (IS) and quadrupole splitting (QS), while no magnetic splitting was detected.

Isomer shift is manifestation of electric monopole interaction between nucleus and its environment being the product of the nuclear charge distribution and the electronic charge density at the nucleus. IS gives a valuable

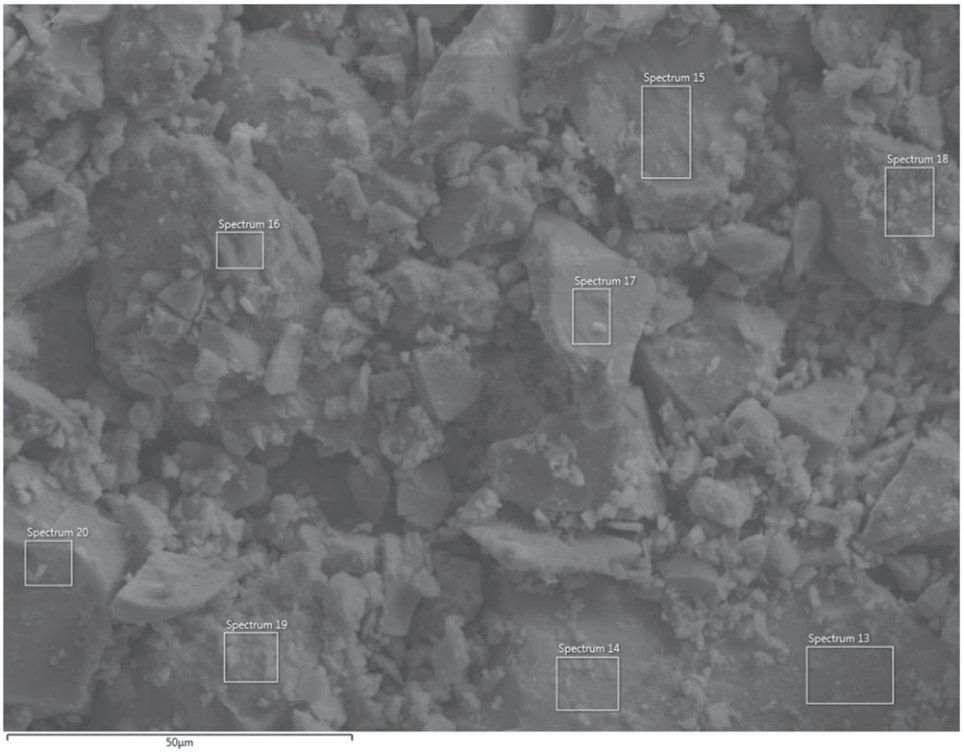

Figure 1. Co-doped SnO_2 powders. The rectangles are the zones of EDX sweeping.

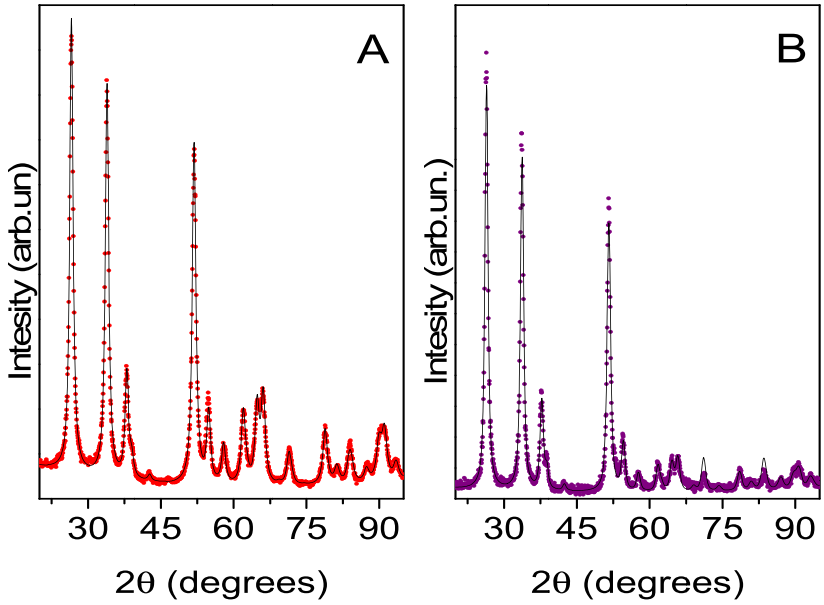

Figure 2. XRD patterns of (A) Mn-doped and (B) Co-doped SnO_2 nanoparticles: the experimental diffractograms (color circles) and Rietveld adjusted curves.

Table 1. Goodness parameters of the fits of XRD patterns.

	SnO_2 + V	SnO_2 + Mn	SnO_2 + Fe	SnO_2 + Co
R_{wp}	8.8%	7.1%	11.2%	16.4%
R_p	6.9%	5.4%	8.3%	12.0%
χ^2	2.23	1.73	1.99	1.64

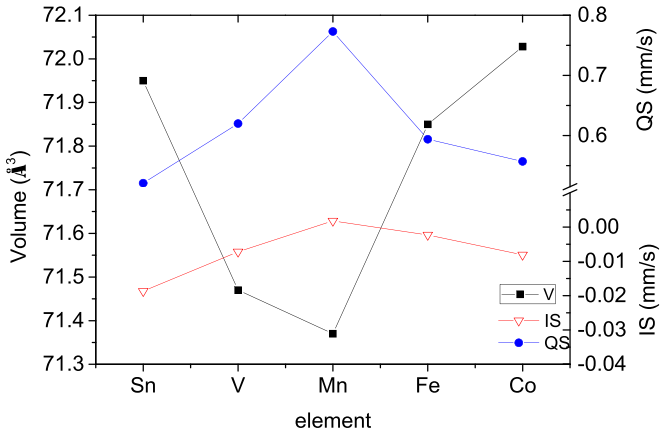

Figure 3. Volume of the rutile lattice in the case of all doped samples and pure SnO_2; IS and QS values from the fitting procedures of all the samples.

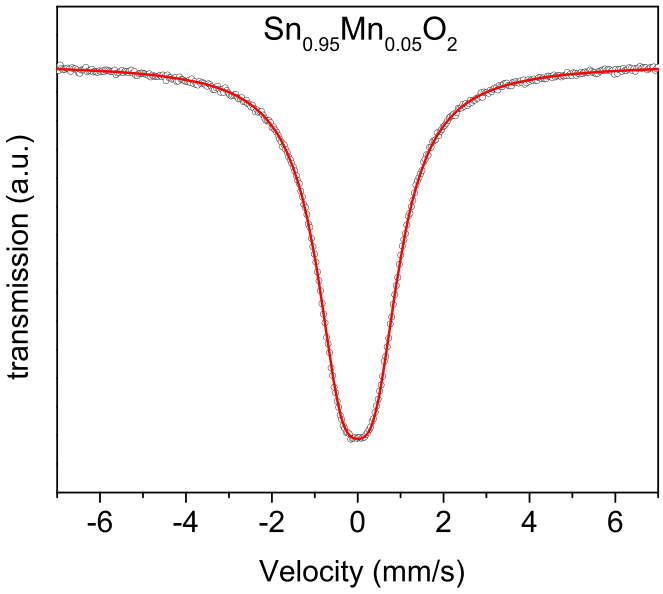

Figure 4. Experimentally acquired Mössbauer absorption spectrum (dots) together with adjusted curve (red solid line).

information about chemical state of the atom probe, that is, oxidation state. QS is manifestation of electric quadrupole interaction between the nuclear quadrupole moment and the tensor of the electric field gradients at the nucleus. Generally, QS is an indicator of the local symmetry around the atom probe.

Mössbauer transmission spectra of the doped-SnO_2 samples are very similar among themselves and were fitted to a doublet, characteristic of a quadrupole electric interaction at nucleus of Sn^{4+} as expected for this type of material [11, 13]. In figure 4, we present only a Mössbauer spectrum (MS) of Mn-doped SnO_2 powders, whereas the fitted Mössbauer parameters of all the samples are gathered in figure 3 (including un-doped SnO_2 taken as a reference).

As it can be noticed, doping SnO_2 with any of four elements influences the values of the hyperfine parameters of the atom probe. It means that Sn is highly sensitive to the presence of the dopant in the samples. This can be another proof of the dopant incorporation to the host SnO_2 matrix. What is interesting to note is that Mn-doped SnO_2 revealed the maximum deviations from the hyperfine parameters of pure SnO_2: the highest values of isomer shift and quadrupole splitting. On the other hand, Co-doped SnO_2 resulted to have a less notorious influence on tin.

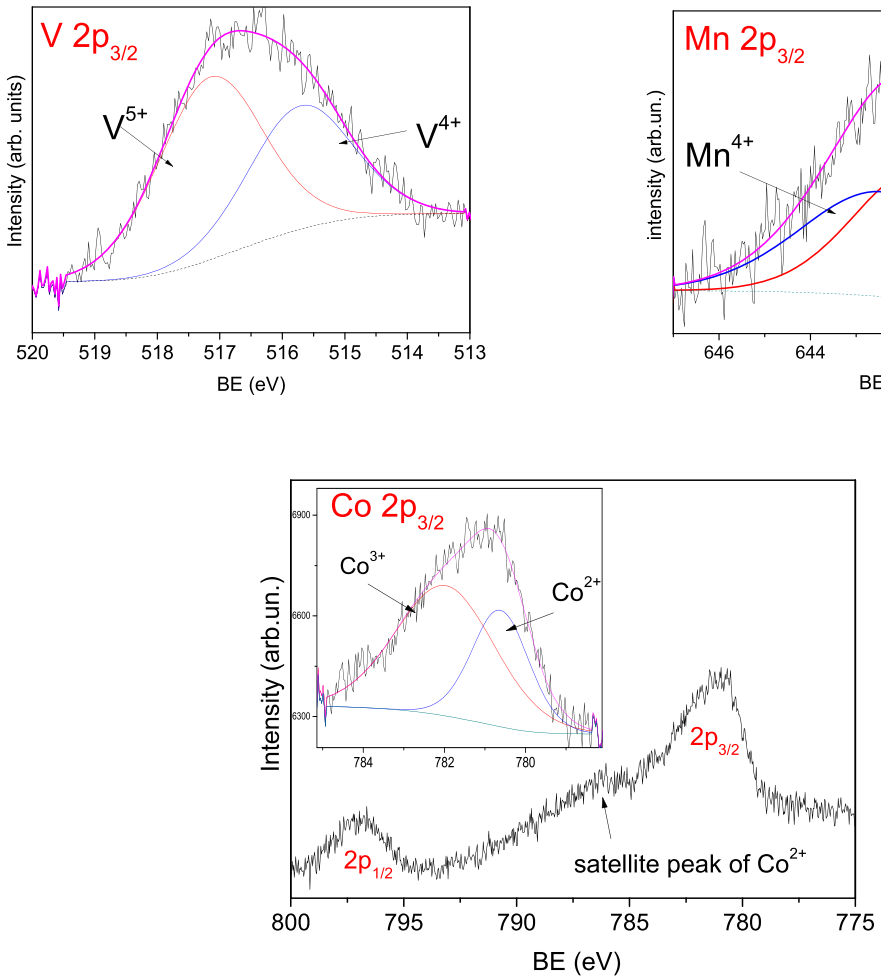

Figure 5. XPS patterns of V, Mn and Co in the samples $Sn_{0.95}V_{0.05}O_2$, $Sn_{0.95}Mn_{0.05}O_2$ and $Sn_{0.95}Co_{0.05}O_2$, respectively.

Table 2. Deconvolution of $3p_{3/2}$ photoelectron peak of V, Mn and Co.

Sample	Ion (BE, eV)	Ion (BE, eV)
SnVO	V4 + (515.71)	V5 + (517.15)
SnMnO	Mn3 + (641.64)	Mn4 + (642.46)
SnCoO	Co2 + (780.68)	Co3 + (782.08)

XPS studies

Dopants (V, Mn, Co)

We have also investigated the oxidation state of the dopants incorporated in SnO_2 structure by x-ray photoelectron spectroscopy (XPS). Relative quantity of different oxidation states for one element can vary from a surface to a core, being generally the state with highest oxidation state more populated on the surface than in the core.

It was revealed (figure 5) that V, Mn and Co were in two distinct chemical states. In particular, vanadium was identified as V^{4+} and V^{5+}, manganese as Mn^{3+} and Mn^{4+}, cobalt as Co^{2+} and Co^{3+}, oxidation state. The results of the deconvolution of the corresponding spectra (binding energies, BE) are shown in table 2, in accordance with those reported in literature [14–16]. Interestingly, in Sb-doped SnO_2, antimony species were in two distinct chemical state: Sb^{3+} and Sb^{5+} [17].

Tin

From figure 6, it can be seen that Sn on the surface of nanoparticles has two binding energies, that is, there are two slightly different environments for Sn atom. The values of binding energies BE_1 are compatible with those reported usually for Sn^{4+} in pure SnO_2 [18]. Whereas BE_2 values are assigned also to Sn^{4+} atom with an oxygen

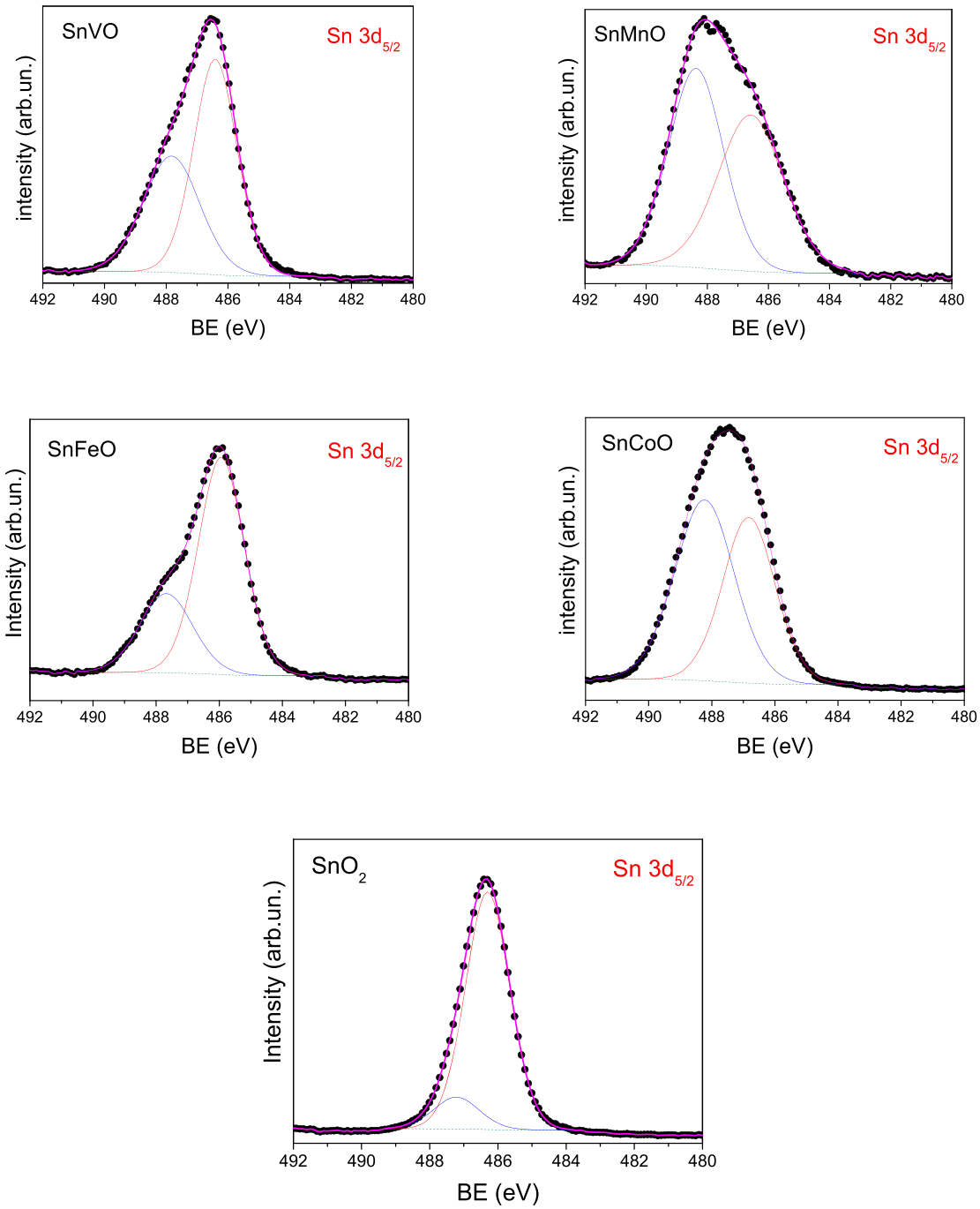

Figure 6. XPS patterns of Sn $3d_{5/2}$ photoelectrons in $Sn_{0.95}V_{0.05}O_2$, $Sn_{0.95}Mn_{0.05}O_2$, $Sn_{0.95}Fe_{0.05}O_2$, $Sn_{0.95}Co_{0.05}O_2$ and SnO_2 samples.

vacancy nearby. An oxygen vacancy can be created to maintain the charge balance when the dopant atom (whose oxidation state is different from 4) replaces for Sn atom. There is a numerous literature suggesting that [19, 20]. A possible appearance of Sn atom with other than 4 + oxidation state, is discarded by MS. In table 3, the deconvolution energies are presented for all the doped and un-doped samples. It can be noticed that the BE_2 component in the doped samples accounts from 30 to 55%, meanwhile in the un-doped sample its contribution is extremely lower (about 12%). In the case of SnO_2, the appearance of such a contribution could be due to the intrinsic defects related to the synthesis process.

Assuming that the dopant substitutes for Sn in octahedral coordination (VI) of the rutile and knowing the dopant's charge, one knows the ionic radius of the dopant (we use the Shannon radius table [21]).

Table 3. Deconvolution of Sn $3d_{5/2}$ photoelectron peak.

Sample	BE1 (eV)	BE2 (eV)
SnVO	486.41 (58%)	487.82 (42%)
SnMnO	486.60 (50%)	488.36 (50%)
SnFeO	485.94 (70%)	487.67(30%)
SnCoO	486.82 (45%)	488.22 (55%)
SnO2	486.3(88%)	487.3 (12%)

Table 4. Values of the ionic radii (angstroms) of Sn, and the doping elements present in the nanoparticles, all for 6-coordination. LS-low spin, HS-high spin.

Sn^{4+}	V^{5+}	V^{4+}	Mn^{4+}	Mn^{3+}	Fe^{3+}	Co^{3+}	Co^{2+}
0.69	0.54	0.58	0.53	0.58 (LS) 0.64 (HS)	0.64	0.54 (LS) 0.61 (HS)	0.65 (LS) 0.74 (HS)

Discussion

For the sake of simplicity of understanding, we have gathered the values of the ionic radii in table 4, we mention in our work, from the Shannon radius table [21].

V-doped SnO_2

Both V^{4+} with the ionic radius 0.58 Å and V^{5+} (0.54 Å) can explain well the decreasing of the lattice volume of V-doped SnO_2, compared with the un-doped one. This is the reason of the intermediated value of QS (0.62 mm s^{-1}) originated by the presence of vanadium in the host of SnO_2 matrix.

Mn-doped SnO_2

In accordance with the XRD results (figure 3), the cassiterite structure in the Mn-doped SnO_2 sample has the smallest lattice volume among the samples here investigated. It can be understood by the fact that the ionic radius of Mn^{4+} (0.53 Å) is considerably smaller than that of Sn^{4+} (0.69 Å). In case of Mn^{3+}, also of a smaller size than Sn^{4+}, the ionic radius can be either of 0.58 Å (for low spin, LS) or 0.645 Å (for high spin, HS). Interestingly, the tin in Mn-doped sample revealed the higher quadrupole splitting (QS $=$ 0.77 mm s^{-1}) value. In other words, the local environment of tin atom is mostly distorted when SnO_2 is doped with manganese.

Fe-doped SnO_2

In case of Fe-doped SnO_2, we assume it is dealt with Fe in 3+ oxidation state (HS). We will argument that in the next section. Its ionic radius, of 0.645 Å, which, again, is smaller than Sn^{4+} ionic radius, explains the volume contraction of Fe-doped SnO_2 sample in comparison with the un-doped one.

Co-doped SnO_2

In accordance with the XRD results, Co-doped SnO_2 powders have the biggest lattice volume among the doped samples, including the un-doped SnO_2. This is an indication of the fact that a bigger ion substitutes for Sn^{4+}. In case of Co^{3+}, the radii are 0.61 Å (HS) and 0.545 Å (LS). From the other hand, Co^{2+} has 0.745 Å (HS) and 0.65 Å (LS). Due to these considerations, only Co^{2+} (HS) can be responsible for the expansion of the lattice of Co-doped SnO_2. This is consistent with the fact that the salt used for doping was $CoCl_2$ where the cobalt clearly is in Co^{2+} state. We believe that in the core of the nanoparticles cobalt remains mainly in the original oxidation state, while in the surface due to the exposition to oxygen, most of the Co get oxidized achieving Co^{3+} oxidation state. From Mössbauer spectroscopy, in Co-doped SnO_2 sample, the tin is at a distorted environment (QS $=$ 0.56 mm s^{-1}) with a quadrupole splitting value close to the one corresponding of the un-doped SnO_2 (0.52 mm s^{-1}).

General remarks

As it is well known, XPS technique is suitable for studying surfaces (nearly 3 nm deep), meanwhile XRD gives information about significantly deeper layers (microns). That means XRD technique 'sees' the whole crystallite (up to 20 nm- size), not its surface. In accordance with the model we propose, SnO_2 doped nanoparticle is a core–shell one, where the core contains the cation with lower oxidation state (for example, here, Co^{2+}), and the shell contains the cation with higher oxidation state (here, Co^{3+}). Because of that mentioned above, XPS spectra

of the dopants (figure 5) do not give a whole quantitative panorama about the populations of the dopants in the doped nanoparticles. Instead, showing the surface state, it gives rather an idea about qualitative model that could take place from our point of view. It should be worth noting, the proposed model is compatible with XRD and MS results.

Moreover, the value of cobalt content, extracted from EDX analysis, reinforces our suggestion about the core–shell model (where the doping elements in the core are of a lower oxidation state) for the system under investigation. Cobalt content in Co-doped SnO_2 nanopowders is somewhat lower that the nominal one, and even though that content (roughly 4 at%) was enough to have the SnO_2 lattice expanded (the only case from those investigated). That is possible only if a bigger ion (than Sn^{4+}) enters predominantly the host lattice. This is the argument in favour of the model proposed (here, Co^{2+}(HS)).

Concerning over the valence state of Fe in SnO_2, we strongly believe that in 5 at% Fe-doped SnO_2 sample, there are no other irons for exception of Fe^{3+}. On one hand, the synthesis of the sample implied $FeCl_3$ salt, where Fe is 3+. It would be improbable to expect Fe^{2+} in such a situation because this would imply reduction of the oxidation state what is very unlikely in nature. So far, we do not find any chemical argument to a favour of the formation of Fe^{2+} during the synthesis by co-precipitation method. On the other hand, in our experiments published previously [11], in 10 and 15 at% Fe-doped SnO_2 nanoparticles, only Fe^{3+} species were detected. This last fact reinforces very strongly our initial guess on Fe^{3+} oxidation state in our sample with 5 at% of Fe. If the sample with 5 at% had irons in 2 + oxidation state, then the samples with more amount of the same species would naturally have more fraction of them in the same oxidation state. In those experiments, no Fe^{2+} ions were detected by the Mössbauer analysis.

A higher isomer shift is related to an increase in the valence electron density (mainly, *s* electrons) at tin nuclei. Undoubtedly, one of the possible contributions to the value of IS is the change of the bonding length due to distinct dopant sizes substituting for Sn. Other possible contribution is well described by Aragon *et al* [8]. They found that the mean particle size reduction of un-doped SnO_2 leaded to an increase in the IS values, ascribing that effect to the generation of *s*-type electrons due to the increase of oxygen vacancies at the nanoparticle surface. Moreover, substituting Sn^{4+} by divalent (for example, Co^{2+}) or trivalent (Fe^{3+}) ions leads to the generation of oxygen vacancies to maintain the charge balance. Interestingly, our un-doped SnO_2 and Co-doped SnO_2 powders have the largest size of the crystallite among all the samples (and the lowest values of the IS). So far, we cannot discard the above-mentioned factors as the ones that could influence the IS.

The increasing of the quadrupole splitting in ionic materials is usually attributed to a more distorted local environment around the probe atom. This is because QS results on the interaction between the nuclear quadrupole moment and the tensor of the electric field gradients at the nucleus. From figure 3, it can be appreciated how the dopant presence impacts the local environments of the Sn in SnO_2 matrix. The main reason is, undoubtedly, the difference in the size of the Sn and the dopant, but, also, the presence of oxygen vacancies could not be discarded as the other source of anisotropic charge density around Sn nucleus. The existence of the oxygen vacancies can be suggested by two binding energies for Sn atom as it was corroborated by the deconvolution of Sn $3d_{5/2}$ photoelectron spectra.

Summarizing, we have shown that in sub-20 nm SnO_2 nanoparticle system when doped nominally at label of 5 at% of V, Mn, Fe or Co the dopant enters the host lattice as can be seen from XRD and MS techniques. XPS suggests the coexistence of V, Mn and Co ions in bi-valence state, where from the suggested model, the lower valence ions are inside of the nanoparticles. While the higher valence ions are more superficial ones. Besides that, XPS gives clear indication of Sn^{4+} with two slightly distinct environments. One of them is in accordance with binding energy of Sn with six nearest oxygen, while the second one is ascribed to the tin atom with an oxygen vacancy nearby. The last could be the consequence of the substitution of Sn by the dopant element of the valence distinct from 4+.

Conclusions

$Sn_{0.95}M_{0.05}O_2$ nanoparticle systems (M: V, Mn, Fe, Co) were investigated by XRD, Mössbauer spectroscopy (MS) and XPS techniques in order to reveal the effect of the dopants on hyperfine parameters of tin in SnO_2 matrix. XRD showed that in all the samples studied, only the diffraction peaks of the rutile structure of SnO_2 without secondary phases were present, which is a sign that the dopants have been incorporated into the host lattice. From Rietveld analysis of the XRD patterns we took into account the modification of the cell parameters and, therefore, the unit-cell volume; this modification is a conclusive evidence that the dopant has been inserted in the lattice of SnO_2. ^{119}Sn transmission MS revealed that the presence of the dopant indeed influences the hyperfine parameters of the tin in the host SnO_2 matrix: both IS and QS values. As it can be seen, there is a clear tendency for the change of the cell volume with IS and QS. With the information about the oxidation states given

by XPS, we found that considering the individual dopant ionic radii (Shannon table), we could explain the modification of the lattice' size of SnO_2 and the hyperfine parameters of tin by the incorporation of the dopants.

Acknowledgments

The authors thank the financial support provided by the Agencia Nacional de Promoción Científica y Tecnológica (ANPCyT) under grant PICT 2016 0364.

The authors also thank Antonela Cánneva and Jorge A. Donadelli (YPF Tecnología S. A.) for XPS measurements and Javier Faig for EDX assistance.

ORCID iDs

V Bilovol https://orcid.org/0000-0002-3363-1840
S Ferrari https://orcid.org/0000-0003-2488-1829

References

[1] Luan H, Zhang C, Li F, Li P, Ren M, Yuan M, Ji W and Wang P 2014 Design of ferromagnetism in Co-doped SnO_2 nanosheets: a first-principles study *RSC Adv.* **4** 9602–7
[2] Ogale S B *et al* 2003 High temperature ferromagnetism with a giant magnetic moment in transparent Co-doped SnO_2 *Phys. Rev. Lett.* **91** 077205
[3] Aragón F H, Coaquira J A H, Cohen R, Nagamine L C C M, Hidalgo P, Brito S L M and Gouvêa D 2012 Structural and hyperfine properties of Ni-doped SnO_2 nanoparticles *Hyperfine Interact.* **211** 77–82
[4] Chen S, Zhao X, Xie H, Liu J, Duan L, Ba X and Zhao J 2012 Photoluminescence of undoped and Ce-doped SnO_2 thin films deposited by sol–gel-dip-coating method *App. Sur. Sci.* **7** 3255–9
[5] Bouzidi C, Elhouichet H and Moadhen A 2011 Yb^{3+} effect on the spectroscopic properties of Er–Yb codoped SnO_2 thin films *J. Lumin.* **131** 2630–5
[6] Bouras K *et al* 2016 Structural, optical and electrical properties of Nd-doped SnO_2 thin films fabricated by reactive magnetron sputtering for solar cell devices *Sol. Energy Mater. Sol. Cells* **145** 134–41
[7] Aragón F H, Gonzalez I, Coaquira J A H, Hidalgo P, Brito H F, Ardisson J D, Macedo W A A and Morais P C 2015 Structural and surface study of praseodymium-doped SnO_2 nanoparticles prepared by the polymeric precursor *J. Phys. Chem.* C **119** 8711–7
[8] Aragón F H, Cohen R, Coaquira J A H, Barros G V, Hidalgo P, Nagamine L C C M and Gouvêa D 2011 Effects of particle size on the structural and hyperfine properties of tin dioxide nanoparticles *Hyperfine Interac.* **202** 1–7
[9] Rumyantseva M N, Safonova O V, Boulova M N, Ryabova L I and Gas'kov A M 2003 Dopants in nanocrystalline tin dioxide *Russ. Chem. Bull.* **52** 1217–38
[10] Punnoose A, Hays J, Thurber A, Engelhard M H, Kukkadapu R K, Wang C, Shutthanandan V and Thevuthasan S 2005 Development of high-temperature ferromagnetism in SnO_2 and paramagnetism in SnO by Fe doping *Phys. Rev.* B **72** 054402
[11] Ferrari S, Pampillo L G and Saccone F D 2016 Magnetic properties and environment sites in Fe doped SnO_2 nanoparticles *Mat. Chem. Phys.* **177** 206–12
[12] Ferrari S, Bilovol V, Pampillo L G, Grinblat F, Saccone F D and Errandonea D 2018 Characterization of V-doped SnO_2 nanoparticles at ambient and high pressures *Mater. Res. Express* **5** 125005
[13] Aragón F H, Villegas-Lelovsky L, Martins J B L, Coaquira J A H, Cohen R, Nagamine L C C M and Morais P C 2017 The effect of oxygen vacancies on the hyperfine properties of metal-doped SnO_2 *J. Phys.* D **50** 1–11
[14] Thian Z M, Yuan S L, He J H, Li P, Zhang S Q, Wang C H, Wang Y Q, Yin S Y and Liu L 2008 Structure and magnetic properties in Mn doped SnO_2 nanoparticles synthesized by chemical co-precipitation method *J. Alloys Comp.* **466** 26–30
[15] Chen W and Li J 2011 Magnetic and electronic structure properties of Co-doped SnO_2 nanoparticles synthesized by the sol-gel-hydrothermal technique *J. App. Phys.* **109** 083930
[16] Cavani F, Trifiro F, Bartolini A, Ghisletti D, Nalli M and Santucci A 1996 SnO_2-V_2O_5 -based catalysts. Nature of surface species and their activity in o-xylene oxidation *J. Chem. Soc. Faraday Trans.* **92** 4321–30
[17] Gržeta B, Tkalčec E, Goebbert C, Takeda M, Takashi M, Nomura K and Jakšić M 2002 Structural studies of nanocrystallne SnO_2 doped with antimony: XRD and Mossbauer spectroscopy *J. Phys. Chem. Sol.* **63** 765–72
[18] Sh S, Gao D, Xu Q, Zh Y and Xue D 2014 Singly-charged oxygen vacancy-induced ferromagnetism in mechanically milled SnO_2 powders *RSC Adv.* **4** 45467
[19] Bilovol V, Mudarra Navarro A M, Rodríguez Torres C E, Sánchez F H and Cabrera A F 2009 Magnetic and structural study of Fe doped tin dioxide *Physica* B **404** 2834–7
[20] Mudarra Navarro A M, Rodríguez Torres C E, Cabrera A F, Weissmann M, Nomura K and Errico L A 2015 *Ab initio* study of the ferromagnetic response, local structure, and hyperfine properties of Fe-doped SnO_2 *J. Phys. Chem.* C **119** 5596–603
[21] Shannon R D 1976 Revised effective ionic radii and systematic studies of interatomic distances in halides and chalcogenides *Acta Cryst.* A **32** 751–67